INVESTIGATE OF PASSIVE FLOW CONTROL METHODOLOGIES USING SST-IDDES

Zhixiang Xiao*, ZhiweiDuan*, Jingbo Huang* and Song Fu*
School of Aerospace, Tsinghua University, Beijing, China, 100084
xiaotigerzhx@tsinghua.edu.cn; dzw05@mails.tsinghua.edu.cn;
huangjb@ tsinghua.edu.cn; fs-dem@tsinghua.edu.cn

Keywords: *vortex generator, turbulence generator, IDDES*

Abstract

In this article, two kinds of passive flow control methodologies, such as vortex generator (VG) and turbulence generator (TG), are investigated using IDDES based on the SST model. The fundamental flows and flow control methodologies are transonic shock wave buffet past a supercritical airfoil with and without VG and hypersonic boundary layer transition flow past a wind tunnel wall with TG, an isolated cylindrical roughness. IDDES combines the wall-modeled large eddy simulation (WMLES) and delayed detached eddy simulation (DDES) and performs well without log-layer mismatch. After applying the flow control methodologies, the buffet region and the pressure fluctuation are greatly suppressed for the supercritical airfoil case and the transition is successfully triggered for the cylindrical roughness case at hypersonic speed.

1 Introduction

The flow control methodologies are widely used in modern air vehicles. They can provide an expanding degree of freedom in the design and optimization process. The performances of economics and environment protection can be greatly improved due to the flow control methodologies, which can suppress the separation, reduce the drag, increase the performance, control the noise, trigger the transition, and so on.

The flow control methodologies include active and passive methods. Active methods can effectively control the flow for the design purpose. However, additional devices and control system, which may lead to increase the weight, cost and complexity, are often needed. Passive flow control methodologies, such as low-profile vortex generator (VG)[1,2] for separation control and turbulence generator (TG) for transition control [3], basically keep the background configuration, but often offer good remedy on overall performances. However, the mechanisms of flow control methodologies are not fully understood, because the VG or TG is almost immerged in the boundary layer. It means that the numerical methods are required to resolve small-scale structures behind the VG or TG. The computations are difficult, expensive and time consumed.

Nowadays, with the rapid increase of computational resource and gradual maturity of really unsteady turbulence prediction methods for high Reynolds number, the mechanisms of passive flow control methodologies are possibly investigated using the resolved turbulence simulation methods, such as direct numerical simulation (DNS), large eddy simulation (LES), and so on.

The most accurate turbulence model can be attributed to the DNS. Overall range of the turbulence scales is directly resolved both in time and space. It requires the spatial and temporal resolution sufficient to predict the smallest eddy motions. DNS is thus the most expensive turbulence prediction approach, which is impossible to be applied to the high Reynolds flows in the recent years.

LES is a powerful tool for resolving the large, energy-containing scale motions that are typically time and geometry dependent. The

reduction in the computational cost as compared with DNS is through introducing some empiricism. The larger energy-containing scale motions are directly computed while the relatively isotropic and universal scale motions are modeled with sub-grid scale (SGS) model. Still, SGS models for the boundary layer and compressible flows are not sufficiently well developed. In fact, LES requires almost similar grid numbers as DNS for high Reynolds number flows near the wall, indicating that LES is equally expensive as DNS in these regions.

Although there are many unanswered questions including the turbulence modeling uncertainty, the Reynolds averaged Navier-Stokes (RANS) equations with various turbulence models are widely employed as appropriate aero-vehicles design approach. The RANS approach had been developed to predict many of the important mean flow features, such as the force, moment and velocity, etc., but it was not intended to simulate the complex unsteady flows, nor pressure fluctuations. Unsteady-RANS (URANS) is not a satisfactory approach to study unsteady turbulence behavior, the large time steps and high-level eddy viscosity always eliminate high frequency small-scale motions.

Limited by computational resource, the combination of LES with RANS can achieve reasonably well in terms of both efficiency and accuracy in computing the flows with massive separation. The modeling strategy of turbulent flows, often referred to as RANS/LES hybrid method (such as DES, originally proposed by Spalart et al. [4], denoted as DES97), has recently become much favored in the study of the unsteady and geometry dependent separated flows. Such hybrid methods combine a high-efficiency turbulence model near the wall, where the flow is dominated by small-scale motions, with a LES-type treatment for the large-scale motions in the flow region far away from the wall. The original DES based on Spalart-Allmaras model [5] achieved widespread acceptance in industrial computational fluid dynamics (CFD) community. However, some inherent shortcomings are identified with the DES97 from its outset and some others are demonstrated through further investigation.

These shortcomings include erroneous activities of the near wall damping terms in LES mode, incursion of LES mode inside boundary layer, grey area and log-layer mismatch. Many of these have been successfully addressed in the later revisions (DDES [6, 7, 8] and IDDES [9]) and some remain. IDDES, which combines the wall-modeled LES (WMLES) and DDES, is chosen as the turbulence or transition simulation model.

The spatial scheme is the upwind Roe scheme with adaptive dissipation, where the originally upwind scheme is taken near the wall and in the irrotational region and the low dissipation is used in the recirculation region. This scheme is applied to keep the numerical robustness and resolve the small-scale of structures as more as possible.

2 Turbulence Simulations and Numerics

To accurately resolve the high Reynolds number flow past roughness, two issues are very important. One is the turbulence simulation model, and the other is the numerical discretization scheme, especially the numerical dissipation level associated with the scheme employed. Furthermore, the combination of the advanced turbulence modeling methods and adaptive dissipation may be more important than either alone.

2.1 IDDES

In this article, IDDES is based on shear stress transport (SST [10]) model. To formulate a DES-type hybrid method based on two-equation k-ω models, modification is required in the destruction term of the turbulent kinetic energy (TKE) transport equation. For RANS, the TKE transport equation can be written as:

$$\frac{\partial(\rho k)}{\partial t}+\frac{\partial(\rho u_j k)}{\partial x_j}=\frac{\partial}{\partial x_j}\left[\left(\mu+\frac{1}{\sigma_k}\mu_t\right)\frac{\partial k}{\partial x_j}\right]+\tau_{ij}S_{ij}-\frac{\rho k^{3/2}}{L_{RANS}} \quad (1)$$

The turbulent length scale for RANS, L_{RANS}, is defined as $k^{0.5}/(\beta^*\omega)$. For IDDES, L_{RANS} is replaced by the length scale of L_{IDEES}.

$$L_{IDDES}=\tilde{f}_d(1+f_e)\times L_{RANS}+(1-\tilde{f}_d)\times L_{LES} \quad (2)$$

Here, the length scale of L_{RANS} is defined before and L_{LES} is defined as $C_{DES}\times\Delta$, where

$\Delta = \max(\Delta x, \Delta y, \Delta z)$. The grid scale is, however, redefined as $\Delta = \min[\max(C_w\Delta_{max}; C_w d; \Delta_{min}); \Delta_{max}]$, where C_w is a constant, d is the distance to the nearest wall, Δ_{min} is taken as $\min(\Delta x; \Delta y; \Delta z)$ and Δ_{max} is equal to $\max(\Delta x; \Delta y; \Delta z)$. Function $\tilde{f}_d$ is defined as $\max[(1-f_{dt}); f_B]$, which is determined by both the geometry part f_B and the flow part $(1-f_{dt})$.

When f_e is equal to 0, L_{IDDES} in Equation (2) can be written as

$$L_{IDDES} = L_{DDES} = \tilde{f}_d \times L_{RANS} + (1-\tilde{f}_d) \times L_{LES} \quad (3)$$

and IDDES reverts to DDES. When f_e is larger than zero and $\tilde{f}_d$ is equal to f_B, L_{IDDES} in Equation (2) is written as

$$L_{IDDES} = L_{WMLES} = f_B(1+f_e) \times L_{RANS} + (1-f_B) \times L_{LES} \quad (4)$$

and IDDES acts in WMLES mode near the wall. The detailed formulations of functions f_B, f_e, f_{dt}, etc., can be found in the original reference.

From Equation (3) and (4), it can be found that IDDES has the WMLES mode, but DDES does not.

2.2 Roe with Adaptive Dissipation

When LES is applied to simulate turbulent flows, the numerical dissipation should be low enough with very fine grids to resolve the appropriate small scales. However, they often suffer from the spurious oscillation due to the coarse grid. The adaptive dissipation scheme, whose dissipation becomes large near the wall and in the irrotational region while very small in the separation region [11, 12, 13], is an appropriate choice. The spatial scheme is taken as the original Roe scheme with 3rd order MUSCL interpolation, coupled with adaptive dissipation by multiplying two functions, σ_1 and σ_2.

$$\overline{F}_{i+\frac{1}{2}} = \frac{1}{2}\Big[F(U_L) + F(U_R) \Big] - \frac{1}{2}\sigma_1 \times \sigma_2 \Big[\Big| \tilde{A}_{inv} \Big| (U_R - U_L) \Big] \quad (5)$$

where $\sigma_1 = \dfrac{\sum(\partial u_i/\partial x_i)^2}{\sum(\partial u_i/\partial x_i)^2 + \|\Omega\|^2}$ is the shock detector[14], which is close to 1 near the shock waves and it approached to zero in other regions. σ_2 is an adaptive dissipation function [12, 13], which is designed to be zero in the separation region and to be one near the wall and in the irrotational region far away from the wall.

2.3 Other Numerics

The in-house code UNITs is in a cell-central finite-volume formulation based on multi-block structured grids. A modified fully implicit LU-SGS with Newton-like sub-iteration in pseudo time is taken as the time marching method when solving the mean flow and the turbulence model equations. The approach is in parallel algorithm using domain-decomposition and message-passing-interface strategies for the platform on PC clusters.

The TKE and specific dissipation rate transport equations are solved, decoupled with the mean flow equations. The production terms are treated explicitly, lagged in time whereas the destruction and diffusion terms are treated implicitly (they are linearized and a term is brought to the left-hand-side of the equations). Treating the destruction terms implicitly helps increase the diagonal dominance of the left-hand-side matrix.

The computations of IDDES start from initial flow-fields obtained with URANS. To obtain second order temporal accuracy, thirty sub-iterations are applied in one physical step.

3 Results and Discussions

3.1 VGs on the Supercritical Airfoil

The modern commercial airplanes always fly at the transonic speed, where the Mach number is typically between 0.75 and 0.9, accompanying the supersonic region on the upper part of the wing. The formation of the shock wave often causes an increase in wave drag. At the same time, the interaction of shock wave and boundary layer (SWBLI) becomes very strong with the increase of Mach number and angle of attack, which causes the separation behind the shock wave and shock wave periodically movement in the streamwise direction, called as buffet.

Buffet badly affects flight stability, control and performance. It was confirmed by the wind channel experiments, flight test and numerical simulations. It is discovered that transonic buffet is highly related to shock wave

oscillation motion on the wing and fluctuating pressure waves in separation induced by SWBLI. As shock wave oscillation motion and surface curvature effect are involved, accurate buffet simulation is a challenge on turbulence prediction, aero-acoustics and aeroelastics. The ordinary buffet control devices are the vortex generators (VG), always observed on the wing of Boeing airplanes, like 737[15], 757 and 777. The VGs have several slices with almost zero thickness.

In this article, the uncontrolled shock wave buffet flow is past supercritical airfoil-OAT15A, which was tested experimentally in ONERA. It was also chosen as a stepping case in EU's 7th framework ATAAC project [16]. The airfoil has a chord (C) of 230mm and a span of 780mm. The maximum thickness is 12.3%C and the trailing edge thickness is about 0.5%C. The Mach number is 0.73 and the angle of attack is 3.5 degrees with strong shock wave buffet and boundary layer separation. Fixed transition is switched on at 7%C on the lower and upper surface. A normalized time step $\Delta t=0.005$ is used to solve unsteady three-dimensional flow.
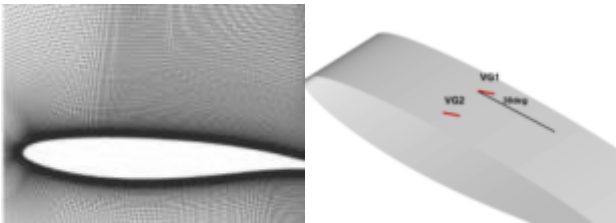

Figure 1 Near fields grids and 2VGs

It has about 7.5 million cells. In the spanwise direction, 65 points are distributed uniformly with intervals of 0.004C, which means that the spanwise length is 0.26C. The first cell height in the normal direction is about 5×10^{-6}C, corresponding to y^+ about 1. In the streamwise direction, grids in and behind shockwave buffet regions and in the wake are locally refined to simulate the buffet and small scale of structures. The far-field boundary has about 10C.

Two VGs with an inclination angle of 30 degrees to the main flow are mounted on the upper surface of the OAT15A before the shockwave. As shown in Figure 1, they are corotating standard VGs with the same

height(H) of the boundary-layer thickness (0.0025C). They are installed at 0.3C from the leading edge. The VGs are rectangular with length L of 8H and zero thickness. The spanwise space between these two VGs is about 36H. The computational grids are based on the uncontrolled case and they are locally clustered near and behind the VGs.

The comparisons of instantaneous and mean flows with and without VGs are presented in Figure 2.

In Figure 2(a), the shock wave can be easily distinguished through the divergence of velocity gradients. It is found that the shock wave around the "clean" airfoil occurs more upstream than that with VGs. The similar tendency can also be found from the shock wave plane, labeled as the grey color, in Figure 2(b). In this figure, instantaneous Q criterion is applied to depict the flow structures.
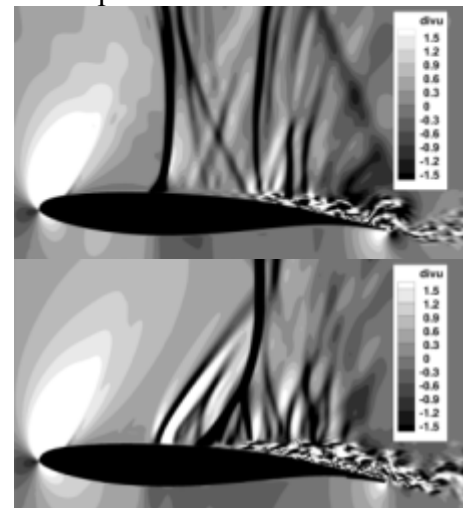
(a)Instantaneous amplitude of velocity gradient

(b)Instantaneous Q criterion

(c) Mean C_p

(d) $C_{p,rms}$

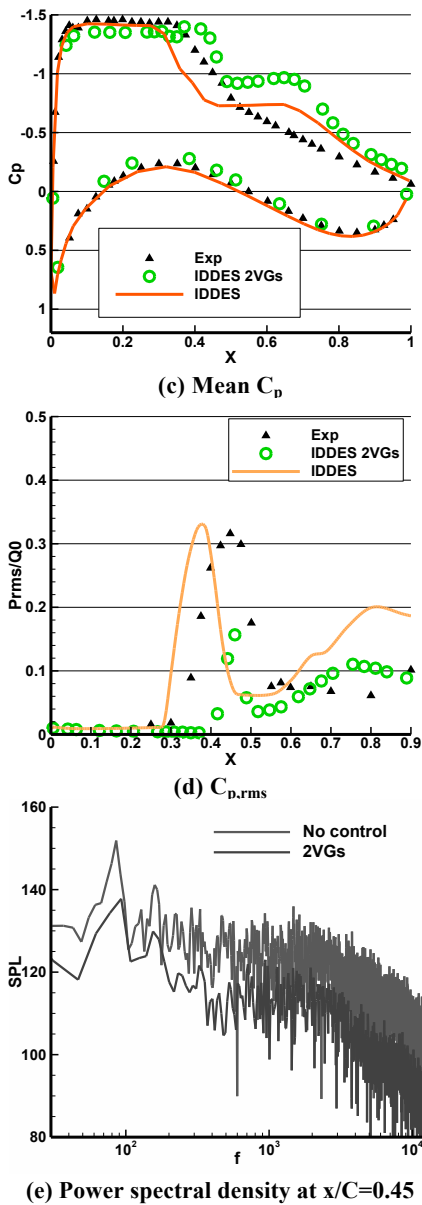**(e) Power spectral density at x/C=0.45**
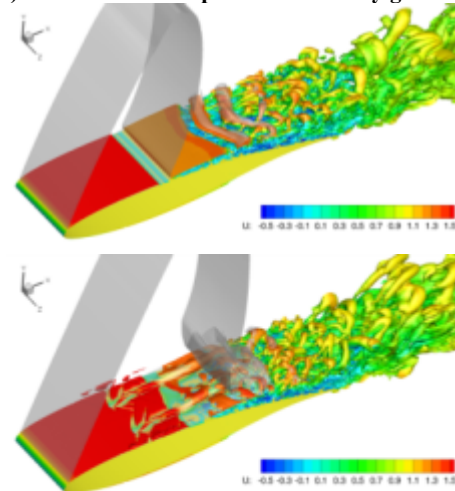
Figure 2 Comparisons of flows without and with VGs

From Figure 2(b), the strong shear layer instability, which breaks down into many small-scale structures, happens behind the shock wave in the streamwise direction. The shear layer around the clean airfoil looks stronger than that with VGs. Due to interaction of the strong streamwise vortex induced by the two VGs, the shear layer breaks down into small-scale structures just at the root of the shock wave with controlled flows.

Figure 2(c) presents the comparisons of mean pressure coefficients with and without the VGs. From these figures, it is found that the VGs can effectively push the shock wave downstream about 0.15C. The approximate roof region in the middle chord is possibly

caused by the strong shear layer or streamwise vortex by the VGs. As a result, the controlled lift coefficients increase from 0.892 to 0.986.

The root mean square of pressure coefficients around the airfoil is presented in Figure 2(d). Our computations can well match the magnitude of $C_{p,rms}$ and the maximum of $C_{p,rms}$ is a little more upstream than measurements around the clean airfoil. After introducing the VGs, the magnitude of the $C_{p,rms}$ becomes smaller and the range of shock wave buffet also becomes weaker.

Figure 2(e) presents the sound pressure level of pressure at x/C=1. The primary frequency is 92Hz, which corresponds to the shock wave buffet frequency. The 2nd frequency is about 1600Hz, which corresponds to shear layer breakdown. The differences between the primary and 2nd frequencies in the two cases are only 6~7 Hz. It indicates that VGs' control does not destroy the self-sustained shock wave boundary layer interaction or change the frequency. About 14 dB decrease of the primary frequency and 11 dB decrease of the secondary frequency by VGs are observed. Thus, it can be concluded that VGs can effectively suppress the shock wave buffet.

3.2 Cylindrical Roughness in Hypersonic Boundary Layer

Wheaton and Schneider [17] experimentally conducted the cylindrical roughness, which triggered transition in quiet hypersonic wind tunnel of Purdue University. According to their report, the diameter of the roughness d is 5.97mm and the height of the roughness h is 10.2mm, which is about 1.2 times of the boundary layer thickness. They also investigated the transition using DNS [18].

In this article, the geometry of wind tunnel wall is not exactly the same with the experiment because its geometry was not reported. Here, the wind tunnel wall is considered as a cylindrical wall, where its diameter is 0.24m, without the divergence. The free-stream Mach number Ma= 6 and the Reynolds number Re= 2.6×10^7/m.

The total cells are about 30 million, the grid scale in the wake region is about 0.4mm (16 points per diameter), and the first point off

the wall in the normal direction is about 20 μm. The near-field grids are presented in Figure 3.
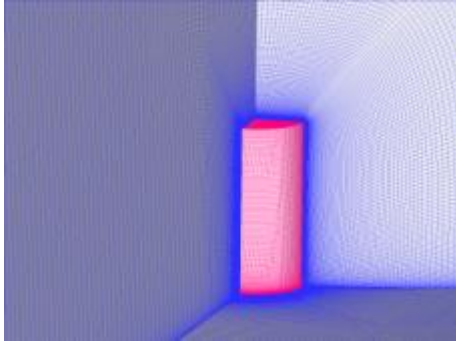

Figure 3Near-field grids past cylindrical roughness

Due to the junction of the wind tunnel wall and the roughness element, the horseshoe vortex can also be easily found before the roughness, shown in Figure 4. From it, the vortices before the cylindrical roughness becomes very small and they develop, evolve and breakdown around the roughness.
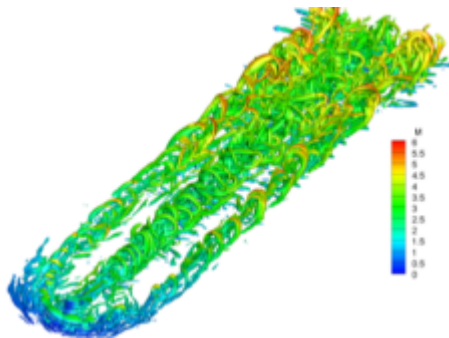

Figure 4 Q-criterion colored by Ma number

Figure 5 and 6 presents the instantaneous density gradient magnitude distribution in the circumferential and normal directions. From these instantaneous flows, the advanced IDDES model coupled with the adaptive dissipation is able to resolve the small-scale structures and explore the transition from laminar to turbulent through analyzing the behavior of small-scale motions. From these figures, the shocklets near the outside of the boundary layer are also easily found. It means that our numerical scheme is robust and successful for capturing both the small-scale structures and shock wave.

The presence of the cylindrical roughness will slow down the main flow. As a result, a low-velocity region occurs in the wake of the roughness. Due to the interaction between the high-velocity out the boundary layer and low-velocity flow in the wake, a very strong shear

layer can be observed near the top of the cylindrical roughness. This shear layer is also unstable and its instability happens behind the roughness, which cause the transition. Because the velocity of main flow is much larger than that in circumferential direction, the vortices in the wake and the horseshoe vortex flow downstream, separately without interactions. They finally interact after 30D after the roughness and the flow becomes turbulent. In this case, the transition in the wake is mainly dominated by shear layer instability and the transition in side region of the roughness is mainly caused by the horseshoe vortex instabilities. Between them, the flow keeps laminar. After the interaction region of vortices in the wake and the horseshoe vortex, the flow becomes turbulent.
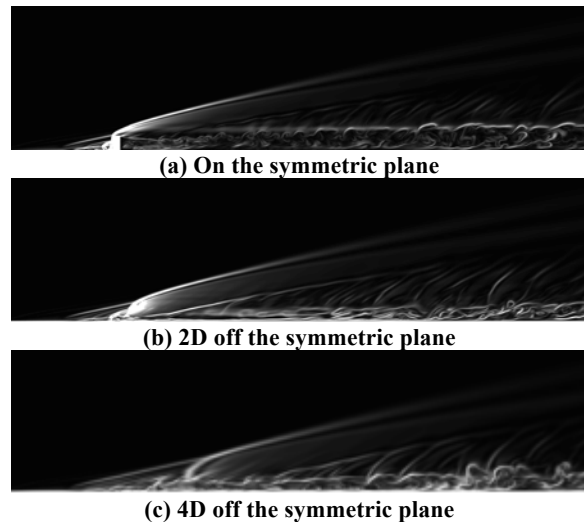

(a) On the symmetric plane

(b) 2D off the symmetric plane

(c) 4D off the symmetric plane
Figure 5 Density Gradient magnitude distributions in the circumferential direction

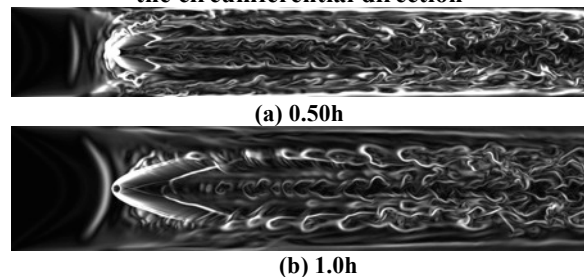**(a) 0.50h**

(b) 1.0h
Figure 6 Magnitude of density gradient at four normal sections

Figure 7 presents the instantaneous and averaged skin friction coefficients on the symmetric plane, corresponding to the shear layer region, and on the 4D off the symmetric plane, corresponding to the horseshoe vortex region. From the distribution of C_f, it's found that the flow becomes turbulent at 0.17m, where

it is about 28D after the roughness. Along the horseshoe vortex, the flow becomes turbulent at 0.24m (about 40D after the roughness) or longer.
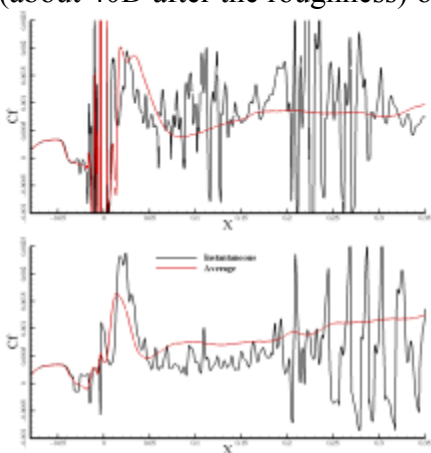

Figure 7 Instantaneous and averaged C_f (on the symmetric and 4D off symmetric plane).

The root-mean-square pressure coefficients normalized by averaged pressure $P_{rms}/<P>$ are able to reflect the local disturbance level of the flow. Figure 8 presents the distribution of $P_{rms}/<P>$ at several positions after the roughness.

(1) In the wake region near the roughness (about 5D downstream), the disturbances are constrained in a relatively narrow region and the strongest disturbance appears in the shear layer region.

(2) At about 10D downstream of the roughness, the disturbance caused by the horseshoe vortex becomes strong and it is almost the same order of that by the shear layer.

(3) At about 20D downstream of the roughness, the disturbance caused by the horseshoe vortex is larger than that by the shear layer and the influencing region becomes higher.

(4) At about 30D downstream of the roughness, the disturbance is mainly dominated by the horseshoe vortex. The disturbance by the shear layer becomes very weak, which means the transition occurs.

(5) At about 40D downstream of the roughness, the disturbance is dominated by the horseshoe vortex and the disturbance by the shear layer can be neglected. It indicates that the flow near the symmetric plane becomes turbulent, while the flow along the horseshoe vortex is also laminar.

(6) At about 50D downstream of the roughness, the disturbance by the horseshoe vortex

becomes weak, which means the flow occurs transition and becomes turbulent.
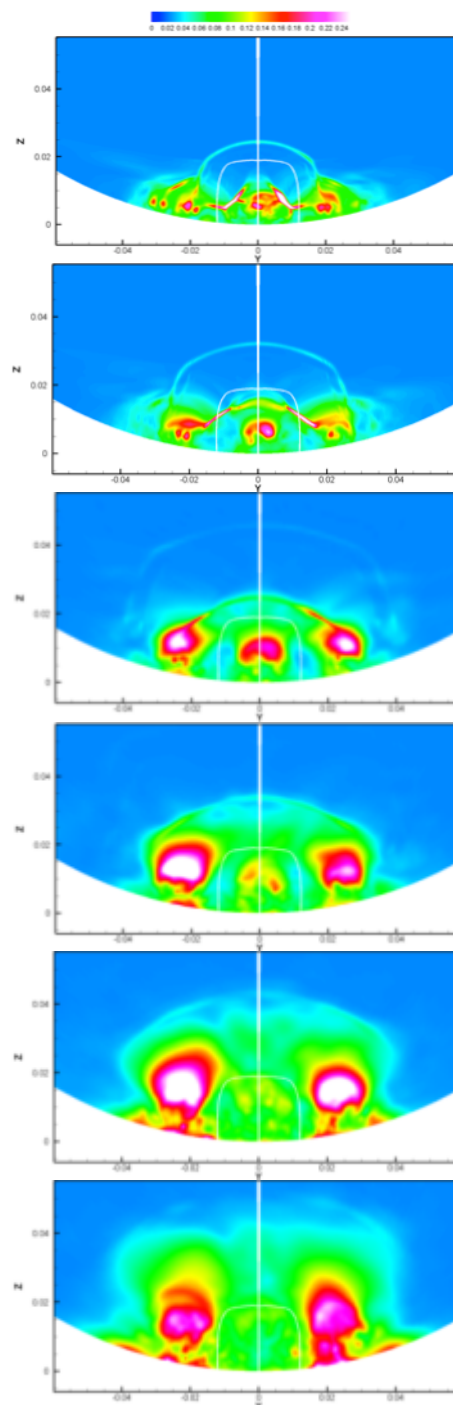

Figure 8 P_{rms} at several positions after the roughness (5/10/20/30/40/50D)

4 Conclusions

In this article, IDDES, a high efficiency and accuracy model, is applied to simulate the benchmark and controlled transonic flows by VGs past the supercritical airfoil (OAT15A) and

the transition flow triggered by a cylindrical roughness in hypersonic boundary layer.

For the case of OAT15A, VGs can greatly suppress the shock wave buffet both in oscillation range and amplitude. The additional advantage is that the lift is increased.

For the roughness case, the cylindrical roughness can successfully trigger the transition in the hypersonic boundary layer. The transition is mainly caused by the shear layer instability and the horseshoe vortex instability.

5 Acknowledgments

References

[1] Yao CS, Lin JC and Allan B, "Flow-Field Measurement of Device-Induced Embedded Streamwise Vortex on a Flat Plate," AIAA Paper 2002-3162, 2002.

[2] Lin J C."Review of Research on Low-Profile Vortex Generators to Control Boundary-Layer Separation,"Progr Aero Sci, 38: 389-420, 2002.

[3] BM Wheaton, SP Schneider, "Roughness-Induced Instability in a Hypersonic Laminar Boundary Layer," AIAA Journal, 50(6), pp. 1245-1256, 2012.

[4] Spalart PR, Jou WH, Strelets M and Allmaras SR, "Comments on the Feasibility of LES for Wings, and on a Hybrid RANS/LES Approach," First AFOSR International Conference on DNS/LES, Aug. 1997, Ruston, LA. Advanced in DNS/LES, edited by Liu, C. and Liu, Z., Greyden Press, Columbus, OH.

[5] Spalart PR and Allmaras SR, "A One-Equation Turbulence Model for Aerodynamic Flows," AIAA paper 92-0439, Jan. 1992.

[6] Spalart PR, Deck S, Shur M, Squares K, Strelets M and Travin A, "A New Version of Detached Eddy Simulation, Resistant to Ambiguous Grid Densities," Theoretical and computational fluid dynamics, 20(3), pp.181-195, May 2006.

[7] Menter FR and Kuntz M, "A Zonal SST-DES Formulation," DES-WORKSHOP, St. Petersburg, July 2003.

[8] Fu S, Xiao ZX, Chen HX, Zhang YF and Huang JB, "Simulation of Wing-Body Junction Flows with Hybrid RANS/LES Methods," Int. J. of Heat and Fluid Flow, 28(6), pp. 1379-1390, July 2007.

[9] Shur M, Spalart PR, Strelets M and Travin A, "A hybrid RANS/LES Approach with Delayed DES and Wall-Modelled LES Capabilities," Int. J. of Heat and Fluid Flow. 29(6), pp.1638-1649, Sep. 2008.

[10] Menter FR, "Two-Equation Eddy-Viscosity Turbulence Models for Engineering Applications," AIAA Journal, 32(8), pp.1598–1605, 1994.

[11] Strelets M, "Detached Eddy Simulation of Massively Separated Flows," AIAA paper 2001-0879, 2001.

[12] Mockett C, "A Comprehensive Study of Detached-Eddy Simulation," Doctoral thesis, Technical University Berlin, 2009.

[13] Xiao ZX, Liu J, Huang JB and Fu S, "Numerical Dissipation Effect on the Massive Separation around Tandem Cylinders," AIAA Journal, 55(5), pp.1119-1136, 2012.

[14] Yoon S, Barnhardt MD and Candler GV, "Simulations of High-Speed flow over an Isolated Roughness," AIAA paper 2010-1573, 2010.

[15] Huang JB, Xiao ZX, Fu S and Zhang M. "Study of Control Effects of Vortex Generators on a Supercritical Wing," Science China-Technological Sciences, 53(8), pp. 2038-2048, 2010/8.

[16] http://cfd.mace.manchester.ac.uk/ATAAC/Web Home.

[17] Wheaton BM, Bartkowicz MD, Subbareddy PK, Schneider SP and Candler GV, "Roughness-Induced Instabilities at Mach 6: A Combined Numerical and Experimental Study," AIAA paper 2011-3248, 2011.

[18] Wheaton BM, Bartkowicz MD, Subbareddy PK, Schneider SP and Candler GV, "Roughness-Induced Instabilities at Mach 6: A Combined Numerical and Experimental Study," AIAA paper 2011-3248, 2011.

Copyright Statement